Journal of Power Sources 248 (2014) 246–252

Contents lists available at ScienceDirect

Journal of Power Sources

journal homepage: www.elsevier.com/locate/jpowsour

Solvothermal synthesis of Fe-doping $LiMnPO_4$ nanomaterials for Li-ion batteries

Lingjun Hu, Bao Qiu, Yonggao Xia*, Zhihong Qin, Laifen Qin, Xufeng Zhou, Zhaoping Liu*

Advanced Lithium Ions Batteries Engineering Laboratory, Ningbo Institute of Materials Technology & Engineering (NIMTE), Chinese Academy of Sciences, Ningbo, Zhejiang 315201, PR China

HIGHLIGHTS

- The Fe-doping $LiMnPO_4$ nanomaterials were synthesized by a solvothermal method.
- The particle morphology could be controlled simply by adjusting the pH values of precursor suspensions.
- The nanoplates along with [010] crystallographic axis with 20–30 nm could deliver the largest discharge capacity.
- Fe doping could significantly increase the initial reversible capacity.

ARTICLE INFO

Article history:
Received 6 July 2013
Received in revised form
9 September 2013
Accepted 11 September 2013
Available online 19 September 2013

Keywords:
Lithium ion batteries
Solvothermal
Cathode materials
Lithium manganese phosphate

ABSTRACT

The Fe-doping $LiMnPO_4$ ($LiMn_{1-x}Fe_xPO_4$, $x \leq 0.5$) nanomaterials are solvothermally synthesized in a mixed solvent of water and polyethylene glycol (PEG). The particle morphology can be controlled simply by adjusting the pH values of precursor suspensions. Electrochemical test shows that $LiMn_{0.9}Fe_{0.1}PO_4$ nanoplates with a thickness of 20–30 nm could deliver the largest discharge capacity, which is attributed to the fast Li^+ diffusion in the diffusion path of [010] crystallographic axis along the short radial direction of the nanoplates. It is demonstrated that Fe doping could significantly increase the initial reversible capacity, cycle performance and rate capability. The first discharge capacities of Fe-doped $LiMnPO_4$ are all above 150 mAh g^{-1} at the discharge rate of 0.05 C. Especially, $LiMn_{0.5}Fe_{0.5}PO_4$ delivers 100% capacity retention with the reversible capacity of 147 mAh g^{-1} at the discharge rate of 1 C, and losses only about 23.4% capacity with the discharge rate varying from 0.1 C to 5 C. The variation of energy density predicts that $LiMn_{0.5}Fe_{0.5}PO_4$ shows the potential application for high-power devices.

1. Introduction

Olive-type $LiMPO_4$ (M = Fe, Mn, Co, Ni etc.) have been extensively investigated as promising cathode materials since the pioneering work of Padhi et al. [1–3]. Among these phosphates, $LiFePO_4$ gets the most attention and has already been commercialized due to its excellent rate capability and preferable safety. However, low operating-potential (~3.5 V *vs.* Li^+/Li), meaning low energy density, limits its application in high-energy devices [4–6]. Recently, to develop the energy density of lithium ion batteries, many researchers have made great efforts to explore a more attractive member of this group. $LiMnPO_4$, which exhibits a higher energy density, is about 20% larger than that of $LiFePO_4$ due to its higher operating voltage (4.1 V *vs.* Li^+/Li). Moreover, compared to other high potential olivine-type cathode materials such as $LiNiPO_4$ (5.1 V *vs.* Li^+/Li) and $LiCoPO_4$ (4.9 V *vs.* Li^+/Li), the 4.1 V intercalation potential of $LiMnPO_4$ is compatible with conventional non-aqueous organic electrolytes of lithium ion batteries [7].

However, $LiMnPO_4$ suffers from poor electronic conductivity and low lithium diffusivity, even much worse than those of $LiFePO_4$, which lead to its low discharge capacity, high polarization and poor rate capability [8,9]. These have become the main obstacles for its practical application in lithium ion batteries. In order to improve the electrochemical performance of $LiMnPO_4$ cathode materials, many attempts have been reported [10–15]. The results confirmed that a great increase in the electrochemical performance when substituted some Mn^{2+} by Fe^{2+} to form the solid solution $LiMn_{1-x}Fe_xPO_4$, and it combines the good rate capability of $LiFePO_4$ and high potential of $LiMnPO_4$ [16–21]. Numerous synthetic methods to obtain $LiMn_{1-x}Fe_xPO_4$ with the improved electrochemical performance have been extensively investigated [22–30]. For example, Hong et al. reported $LiMn_{0.8}Fe_{0.2}PO_4$ prepared by a

* Corresponding authors. Tel./fax: +86 574 8668 5096.
E-mail addresses: xiayg@nimte.ac.cn (Y. Xia), liuzp@nimte.ac.cn (Z. Liu).

0378-7753/$ – see front matter © 2013 Elsevier B.V. All rights reserved.
http://dx.doi.org/10.1016/j.jpowsour.2013.09.048

conventional solid-state method could deliver a specific capacity of 138 mAh g^{-1} at 0.1 C [26]. Chen et al. have synthesized $LiMn_{1-x}Fe_xPO_4$/C on the basis of $FePO_4 \cdot 2H_2O$ nanocrystallites, and the samples with $x = 0.25$ have an improved discharge capacity of about 130 mAh g^{-1} at 0.05 C, which is mainly attributed to iron substitution, the appropriate Mn/Fe ratio, and the well-ordered crystal structure of raw materials [28]. Saravanan et al. have succeeded in synthesizing nanoplates of $LiMn_{1-x}Fe_xPO_4$ using a simple solvothermal method. Especially, $LiMn_{0.5}Fe_{0.5}PO_4$/C composite materials exhibited a reversible capacity of 121 mAh g^{-1} at 0.1 C [27]. From above results, it is also confirmed that the electrochemical performance of $LiMn_{1-x}Fe_xPO_4$ cathode materials strongly depends on the synthetic method.

More recently, it is believed that particle morphology is also a key factor that affects the discharge capacity of olivine-type cathode materials [31–37]. Ceder et al. confirmed that lithium ions can move easily along the *b*-axis in the olivine structure due to the low activation barrier along this direction [38]. Recently, Kanamura et al. found the value of pH in the $LiFePO_4$ precursor was of importance to control the morphology, especially plate-like crystal growth [31]. In addition, Wang et al. also revealed that the sample with platelet morphology (only ~30 nm thick oriented in the *b* direction) presented a good rate capability [25]. It exhibited a specific capacity of 145 mAh g^{-1} at C/20, 141 mAh g^{-1} at C/10 and 113 mAh g^{-1} at 1 C. In our previous work, we have successfully synthesized $LiMnPO_4$ [36] and $LiFePO_4$ [37] cathode materials with certain morphology and nanoscaled particles using solvothermal method, and confirmed that $LiMnPO_4$ thin nanoplates display the largest specific capacity, compared with $LiMnPO_4$ thick nanoplates and nanorods [36]. Under the inspiration of these successes, we speculated that it would be possible to synthesize $LiMn_{1-x}Fe_xPO_4$ with the greatly enhanced electrochemical performance using solvothermal method.

Herein, we reported $LiMn_{1-x}Fe_xPO_4$ (with $x = 0$, 0.1, 0.2, 0.3, 0.4, 0.5) nanoparticles synthesized through solvothermal method. The studies include two aspects. On one hand, efforts were tried to find out the optimal pH value of solvothermal reaction system. On the other hand, $LiMn_{1-x}Fe_xPO_4$ ($x = 0$, 0.1, 0.2, 0.3, 0.4, 0.5) were synthesized under selected condition and their electrochemical performances were discussed in detail. To improve the conductivity, a small quantity of carbon was coated on materials, and the element analysis showed that carbon contents in the final cathode materials were *ca.* 2.7 wt. %.

2. Experimental

2.1. Sample synthesis

$LiMn_{1-x}Fe_xPO_4$ ($x = 0$, 0.1, 0.2, 0.3, 0.4, 0.5) nanoparticles were prepared by solvothermal method, which have been reported for the synthesis of $LiMnPO_4$ and $LiFePO_4$ in our previous work [36,37]. First, polyethylene glycol 400 (PEG 400) was mixed with H_3PO_4 (1 mol L^{-1}), and then LiOH (1 mol L^{-1}) solution was dropwise added to the above mixture with vigorous stirring to regulate the pH value of the system. In this work, the pH value was set as 9, 11, 12.5, for purpose of controlling the morphology of products. After that, $MnSO_4$ (0.5 mol L^{-1}) and $FeSO_4$ (0.5 mol L^{-1}) solutions were slowly introduced into the system in sequence under stirring. The suspension obtained above was then taken in a Teflon lined stainless steel reaction vessel, which was subsequently autoclaved in an oven at 180 °C for 12 h after sealed tightly. After the vessel was allowed to cool down to ambient temperature, the claybank products obtained were collected and washed with ethanol and water each for several times, then dried under vacuum at 80 °C for 12 h. In the above processes, H_3PO_4, $MnSO_4$ and $FeSO_4$ were used in the molar ratio of $1:(1-x):x$. As LiOH was added to adjust the pH value of the system, the molar ratio of Li:(Mn + Fe) in the precursor was about 3:1.

Herein, carbon-coating was carried out via two steps: Firstly, $LiMn_{1-x}Fe_xPO_4$ and sucrose ($LiMn_{1-x}Fe_xPO_4$:sucrose = 9:1, weight ratio) were mixed using planetary ball milling containing appropriate ethanol at 350 rpm for 4 h with a weight ratio of sample: ball = 1:20; secondly, the mixture was annealed at 600 °C for 4 h in an Ar atmosphere. The carbon contents of all the final cathode materials were *ca.* 2.7 wt. % from the element analysis (CHNS/O Elemental Analyzer, PerkinElmer).

2.2. Structure and morphology characterizations

The as-prepared products were characterized by X-ray powder diffraction (XRD, D8 Advance diffractometer, Cu Kα radiation). Morphology was examined using field emission scanning electron microscopy (FESEM) (S-4800, Hitachi) and high-resolution transmission electron microscopy (HRTEM) (Tecnai F20, FEI).

2.3. Electrochemical measurements

Electrochemical properties of the $LiMn_{1-x}Fe_xPO_4$ ($x = 0$, 0.1, 0.2, 0.3, 0.4, 0.5) electrodes were measured after assembling them into coin cells (type CR2032) in an argon-filled glove box using lithium metal as the anode and Celgard 2502 as the separator. The cathode was prepared by spreading a mixture of active material (80 wt. %), acetylene black (15 wt. %), and poly (vinylidene fluoride) binder (5 wt. %) dissolved in *N*-methyl pyrrolidone onto an aluminum foil current collector. The thickness of the electrode was about 20 μm and the loading density of active material on the electrode was about 2.5 mg cm^{-2}. The electrolyte (Zhangjiagang Guotai-Huarong New Chemical Materials Co., Ltd., P. R. China), consists of a solution of 1 M $LiPF_6$ in a mixture of ethylene carbonate/dimethyl carbonate (3:7 vol. %). The coin-typed cells were tested in a voltage range of 2.0 V–4.5 V (*vs.* Li^+/Li) using a constant-current constant-voltage (CC–CV) protocol at various rates with potentiostatic steps at the cutoff potential on a battery tester (LAND-CT2001A, Jinnuo Wuhan Co., Ltd., P. R. China). Cyclic voltammetry (CV) measurements were carried out on an Autolab83710 at a scanning rate of 0.1 mV s^{-1} with the voltage ranging from 2.0 V to 4.6 V. All the tests were conducted at constant temperature (25 °C) and the forming current was 0.05 C.

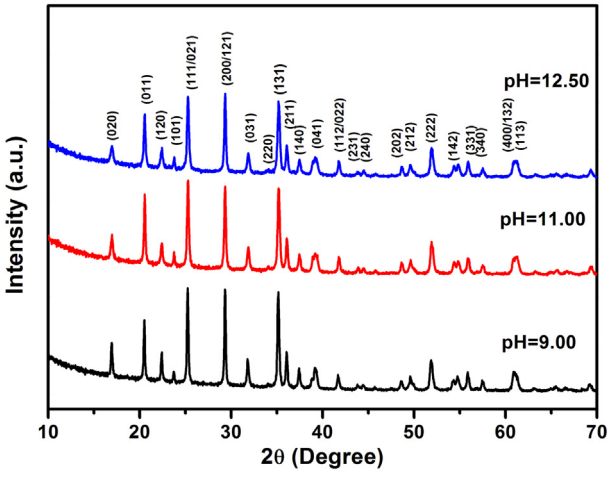

Fig. 1. XRD patterns of $LiMn_{0.9}Fe_{0.1}PO_4$ synthesized at different pH values.

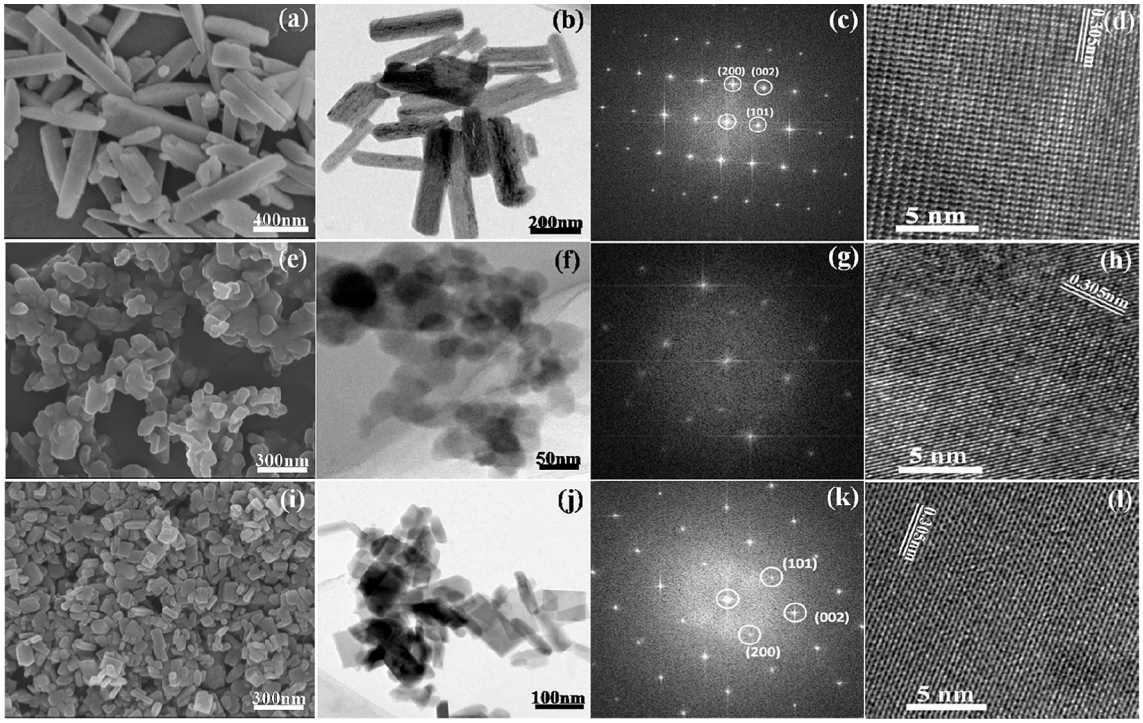

Fig. 2. SEM images, TEM images, SAED patterns of $LiMn_{0.9}Fe_{0.1}PO_4$ synthesized at different pH value of the reaction systems: a)–d) pH = 9; e)–h) pH = 11; i)–l) pH = 12.5.

3. Results and discussion

3.1. The effect of pH value of the reaction suspension

In order to obtain the $LiMnPO_4$ with different morphology and particle size, the pH value of the reaction suspension was adjusted. Fig. 1 shows the XRD patterns of the $LiMn_{0.9}Fe_{0.1}PO_4$ samples synthesized under different pH values with 9, 11, and 12.5. It can be see that the sharp diffraction peaks of all samples could be clearly indexed as orthorhombic olivine with *Pnmb* space group (JCPDS No. 74-0375) and no obvious impurity was detected. This indicates that $LiMn_{0.9}Fe_{0.1}PO_4$ of high crystallinity and pure phase could have been successfully synthesized within the pH range of 9–12.5.

The morphology of as-prepared samples could be controlled simply by adjusting the pH values of suspension. Nanorods (Fig. 2a, b) and nanoplates (Fig. 2i, j) were achieved when the pH values were 9 and 12.5, respectively. The former is mainly 50–100 nm in brachy axis size while the length size has a wider range, and the latter is *ca.* 20–30 nm in thickness and *ca.* 70–100 nm in radial dimension with relatively narrower particle size distribution. The higher the value of pH, the more excess the Li ions in the suspension. In recent reports, it has been demonstrated that the excess Li was favorable for attaining small particle size for $LiFePO_4$ and $LiMnPO_4$ [39,40]. However, the sample synthesized at pH = 11 presents to be 20–40 nm nanoparticles with severe aggregation (Fig. 2e, f). Moreover, the diffraction patterns of both nanorods (Fig. 2c) and nanoplates (Fig. 2k) are regularly distributed spots in a certain way, indicating high crystallinity of particles. The growth direction of particles (Fig. 2d, l) is similar to the pristine ones [36], which have been clarified in details to do a positive effect on shortening the diffusion path of Li^+. Diffraction dots (Fig. 2g) of sample synthesized with pH value of 11.0 are not in a distinct rule-based way. And it indicates low crystallinity of particles with indistinct lattice fringe image.

In addition, after ball-milling and calcining at 600 °C for 4 h, the morphology of carbon-coating $LiMn_{0.9}Fe_{0.1}PO_4$ ($LiMn_{0.9}Fe_{0.1}PO_4$/C) (Fig. 3) differs from the pristine $LiMn_{0.9}Fe_{0.1}PO_4$. The crystals all exists different degree of growth compared to the primitive ones. Nanorods (pH = 9, Fig. 3a) and nanoparticles (pH = 11, Fig. 3c) have grown and aggregated remarkably, while nanosheets change slightly and still have good dispersion, indicating that plate-like shape may be more stable than other shapes.

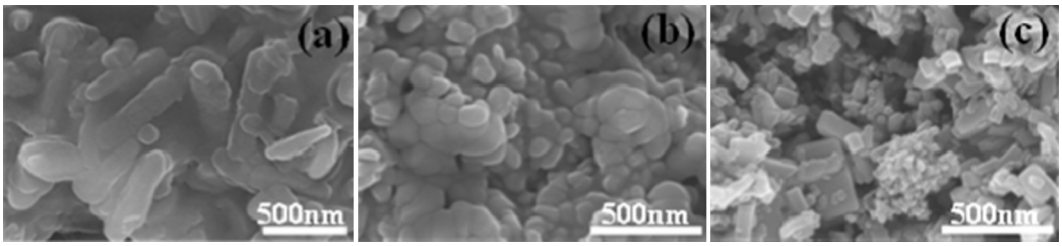

Fig. 3. Field emission scanning electron microscopy (FESEM) images of $LiMn_{0.9}Fe_{0.1}PO_4$/C synthesized at different pH value of the reaction systems: a) pH = 9; b) pH = 11; c) pH = 12.5.

In order to find out the optimal pH value, the electrochemical properties of above three samples were evaluated. From the first charge–discharge curves (Fig. 4a), the initial discharge capacity of three samples is 53 mAh g^{-1} (pH = 9), 139 mAh g^{-1} (pH = 11) and 155.5 mAh g^{-1} (pH = 12.5), respectively. All samples exhibit a plateau centered at ~4.1 V (Mn^{2+}/Mn^{3+}) during charge and discharge, the length of which has correlation with the pH value. In addition, the profiles of the samples synthesized at pH = 11 and pH = 12.5 both show an additional small plateau at ~3.5 V, which should be related to Fe^{2+}/Fe^{3+} redox couples. However, the sample synthesized at pH = 9 seems to be too low capacity to come up with the plateau at ~3.5 V. Fig. 4b shows the cycling performance of the three kinds of $LiMn_{0.9}Fe_{0.1}PO_4/C$, which measured at 0.2 C–1 C for charge and discharge. Reversible capacity of the first cycle is 42.5 mAh g^{-1}, 99 mAh g^{-1}, 128 mAh g^{-1} corresponding to $LiMn_{0.9}Fe_{0.1}PO_4/C$ synthesized at pH = 9, 11, and 12.5, respectively. After 30 cycles, their capacity retentions are 113.7%, 85.6%, 93.7% respectively. Fig. 4c exhibits the rate capability of the prepared $LiMn_{0.9}Fe_{0.1}PO_4/C$. In the case of $LiMnPO_4$, it has been reported that not only solid-state diffusion of Li^+ but also the crystallographic structural change give significant effects on the charge–discharge rate capability [41]. It is clear that the sample prepared at pH = 12.5 shows the best rate capability among these samples, as shown in

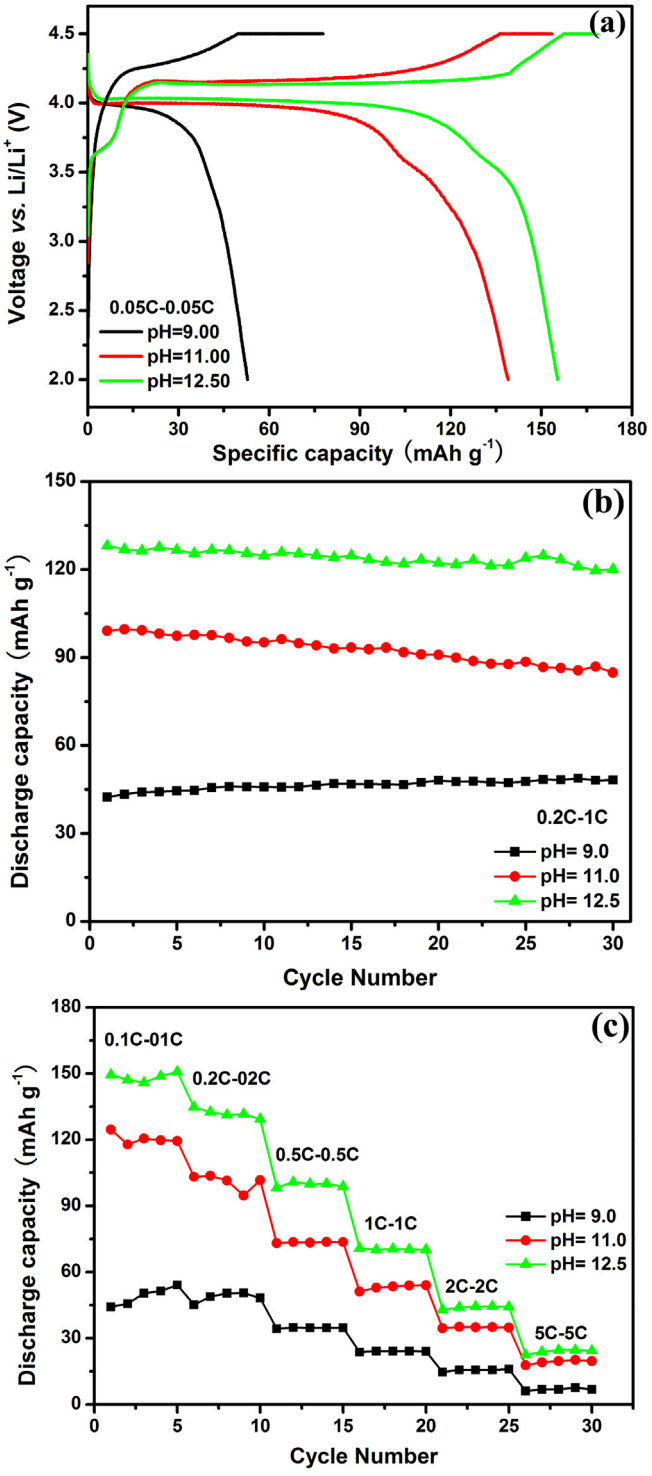

Fig. 4. Electrochemical performance of $LiMn_{0.9}Fe_{0.1}PO_4/C$: a) the first charge/discharge curves of $LiMn_{0.9}Fe_{0.1}PO_4/C$; b) cycling performance of $LiMn_{0.9}Fe_{0.1}PO_4/C$; c) rate capability of $LiMn_{0.9}Fe_{0.1}PO_4/C$.

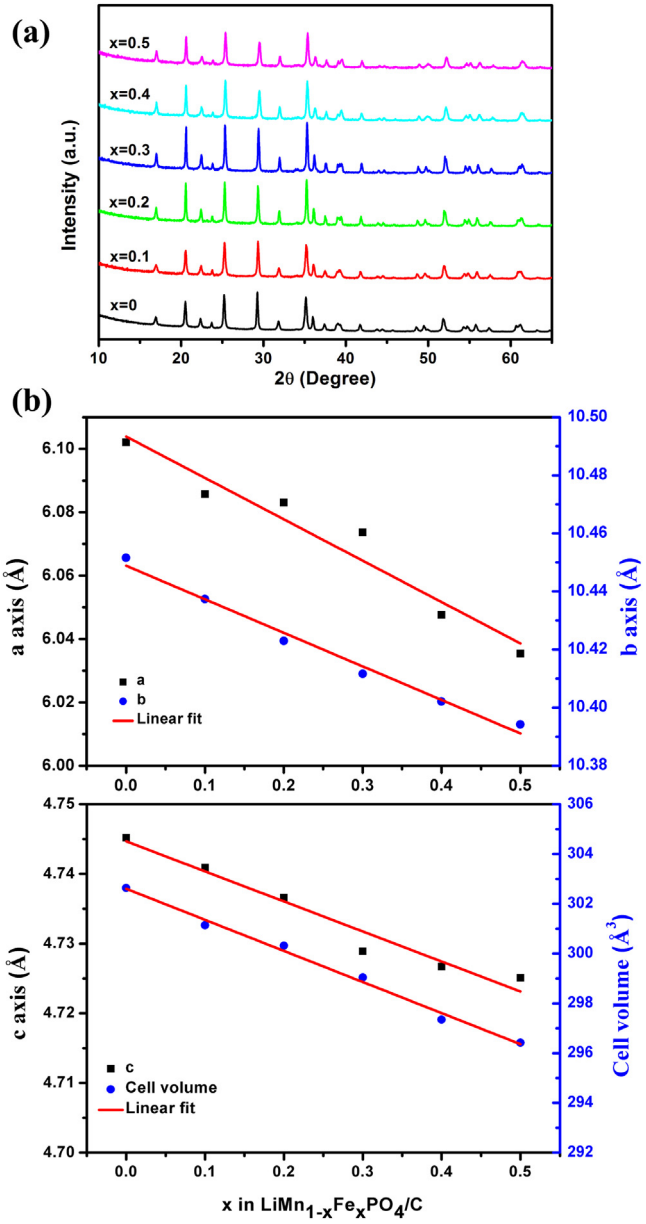

Fig. 5. a) XRD pattern of $LiMn_{1-x}Fe_xPO_4$ samples (x = 0, 0.1, 0.2, 0.3, 0.4, 0.5); b) Calculated lattice parameters and unit-cell volume *vs.* x in $LiMn_{1-x}Fe_xPO_4$ samples.

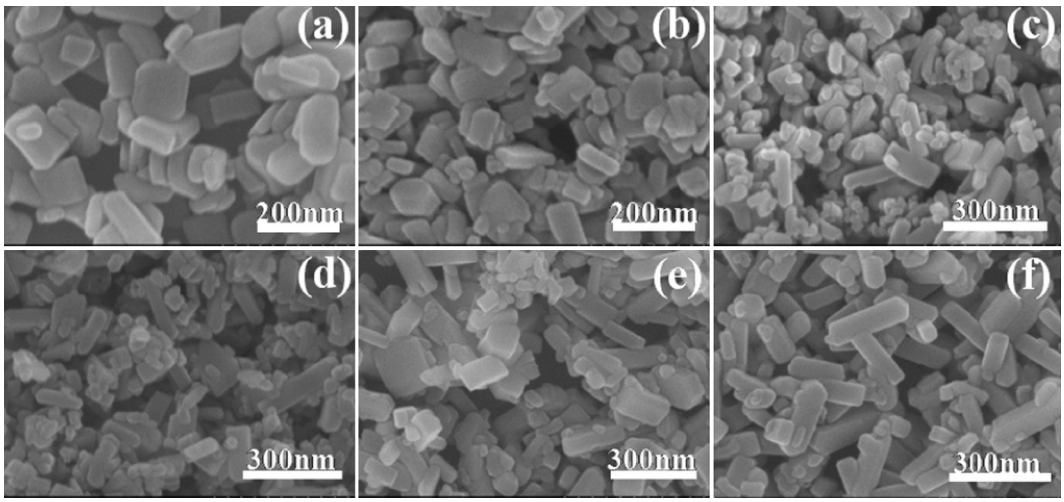

Fig. 6. a) The first charge/discharge curves of $LiMn_{1-x}Fe_xPO_4$/C; b) cyclic voltammograms of $LiMn_{1-x}Fe_xPO_4$/C.

Fig. 2(c, g, k). Therefore, the reason above has been confirmed that the optimal pH value is 12.5.

3.2. The effect of iron doping content

To take step further, $LiMn_{1-x}Fe_xPO_4$ ($x = 0$, 0.1, 0.2, 0.3, 0.4, 0.5) were prepared to study the impact of Fe content while the pH value was controlled at 12.5. The XRD patterns of $LiMn_{1-x}Fe_xPO_4$ are presented in Fig. 5a, illustrating that all samples have a single olivine phase with space group *Pmnb* and no feature peaks of impurities are observed. All the diffraction peaks move to higher angles in a continuous fashion with increasing concentrations of Fe. In order to obtain more detailed information for the structure of these samples, lattice parameters and unit-cell volume were calculated and plotted as a function of Fe content in Fig. 5b. As expected, the unit cell shrinks continuously as Fe is introduced into the system and the shape of the curve is expressed as one continuous line, which can be attributed to smaller radius of Fe^{2+} (0.92 Å) than that of Mn^{2+} (0.97 Å) [26]. These data confirmed that Fe was doped into the lattice structure of $LiMnPO_4$ successfully with all setting content, and the formed $LiMn_{1-x}Fe_xPO_4$ was a true solid solution of $LiMnPO_4$ and $LiFePO_4$ as demonstrated by XRD patterns.

The SEM images of these samples were characterized and shown in Fig. 6, where the morphology of pure $LiMnPO_4$ comes to be uniform nanoplates. We note that Fe-doped samples have smaller primary particle size than pure $LiMnPO_4$, which may be beneficial to the electrochemical performance. Moreover, these samples contained both smaller nanoparticles and nanoplates. Compared to the carbon-coating samples (Fig. 7), the morphology has little change, indicating that the coating process just has slight impact on the final products and the electrochemical performances of samples, which is consistent with the above conclusion.

Electrochemical performances of $LiMn_{1-x}Fe_xPO_4$/C ($x = 0$, 0.1, 0.2, 0.3, 0.4, 0.5) were also measured. Fig. 8a shows the first charge–discharge curves of six samples. Two plateaus centered at ~3.5 V and ~4.1 V separately related to Fe^{2+}/Fe^{3+} and Mn^{2+}/Mn^{3+} redox couples are presented for Fe-doped samples. The length of plateau at ~3.5 V becomes much flatter and longer as the Fe amount increases, which also verifies that Mn-site has been successfully partially substituted by Fe. It indicates that Fe substitution conducts a positive impact on two phase transformation during both charge and discharge reaction. Peaks in the CV test (Fig. 8b) come to be proof to the above statements. Both oxidation and reduction peaks for Mn^{2+}/Mn^{3+} and Fe^{2+}/Fe^{3+} couples grow

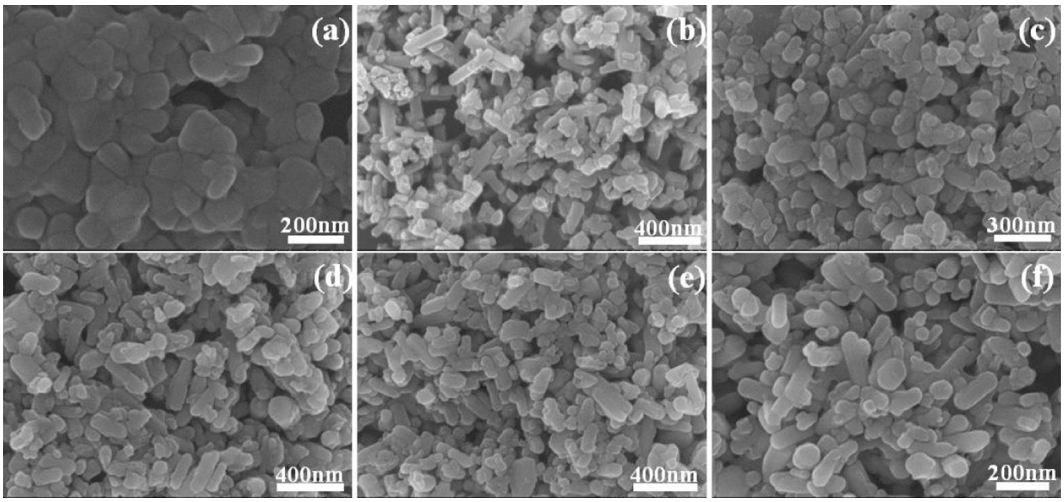

Fig. 7. SEM images of $LiMn_{1-x}Fe_xPO_4$ with carbon coating: a) $x = 0$; b) $x = 0.1$, c) $x = 0.2$; d) $x = 0.3$; e) $x = 0.4$; f) $x = 0.5$.

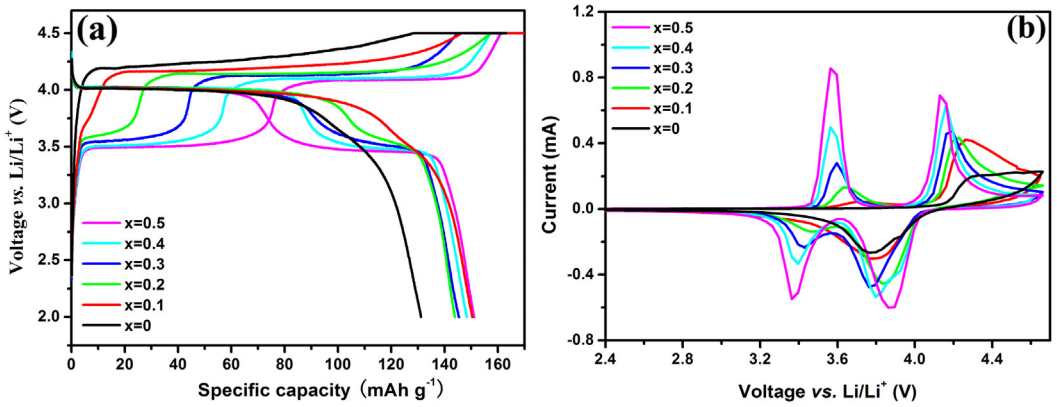

Fig. 8. a) The first charge/discharge curves of $LiMn_{1-x}Fe_xPO_4/C$; b) cyclic voltammetry of $LiMn_{1-x}Fe_xPO_4/C$.

sharper and the intensity of peaks for Fe^{2+}/Fe^{3+} gradually increases. This could be attributed to an improvement in kinetics of the lithium intercalation/deintercalation at the electrode/electrolyte interface and/or the rate of lithium diffusion in the lattice, with the increasing of the content of Fe.

Cycling performance of $LiMn_{1-x}Fe_xPO_4/C$ was also evaluated at 0.2 C for charging and 1 C for discharging (Fig. 9). After 100 cycles, reversible capacity is 57 mAh g^{-1}, 107 mAh g^{-1}, 117 mAh g^{-1}, 124 mAh g^{-1}, 138 mAh g^{-1}, 147 mAh g^{-1}, corresponding to $x = 0, 0.1, 0.2, 0.3, 0.4, 0.5$, respectively. Obviously, Fe-doped samples still show much higher reversible capacity than the pure one. In addition, it is worthy of noting that the capacity retentions of samples go up with increasing the content of Fe, as shown in Fig. 9b. For example, the high capacity retention, corresponding to the ratio of the initial and 100th discharge capacity, is nearly100% for $LiMn_{0.5}Fe_{0.5}PO_4/C$ sample, which is much higher than that of $LiMnPO_4/C$ (75%). Jo et al. reported similar result that Fe-doped could suppress the surface side reactions of the bulk, restrain the dissolution of Mn^{2+}, resulting in better capacity retention [30].

The rate capability of $LiMn_{1-x}Fe_xPO_4/C$ was measured in a CC–CV mode with the same charging/discharging rate as shown in Fig. 9c. The rate capability of $LiMn_{1-x}Fe_xPO_4/C$ has an obvious improvement with increasing the content of Fe. It is seen that $LiMn_{0.5}Fe_{0.5}PO_4/C$ has an excellent rate capacity and still has a discharge capacity of more than 120 mAh g^{-1} even at the 5 C rate, which is much better than the material with same Fe amount as

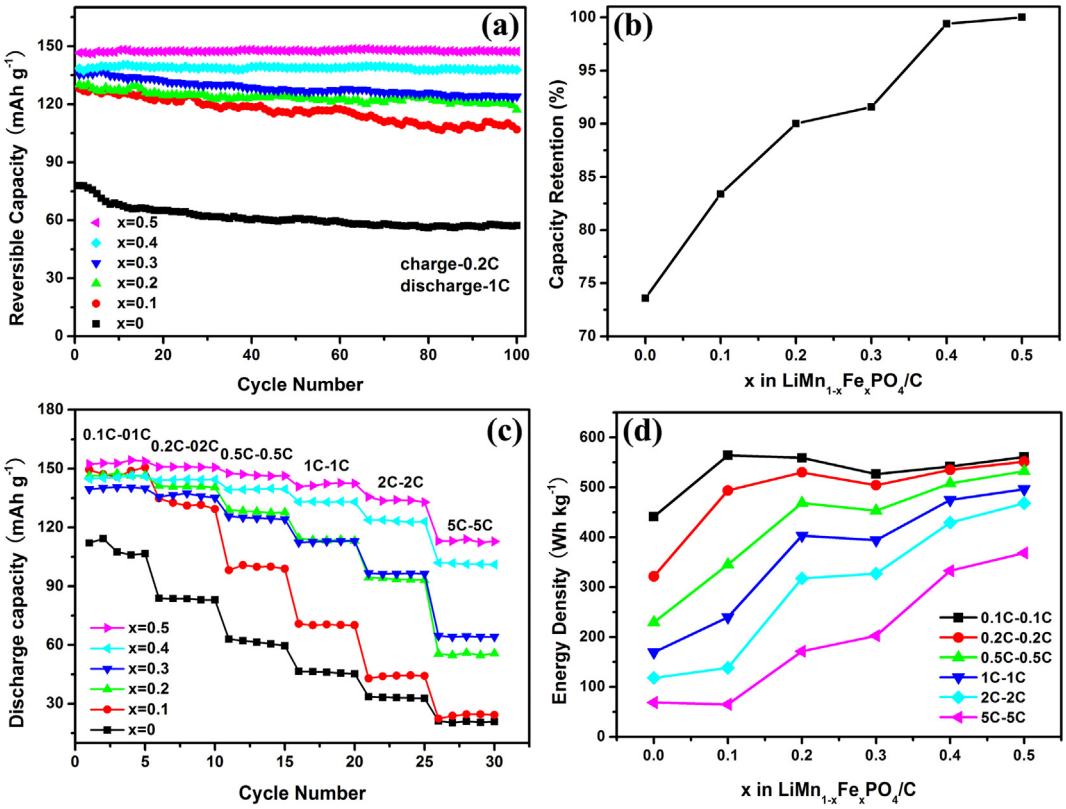

Fig. 9. Cycling performance and rate capability of $LiMn_{1-x}Fe_xPO_4/C$: a) reversible capacity of different cycle number; b) the capacity retention; c) reversible capacity at different rates; d) energy density at different rates.

reported in previous literature [27]. Fig. 9d illustrates how the energy density performs at different rates. At the low rate of 0.1 C and 0.2 C, $LiMn_{0.9}Fe_{0.1}PO_4$/C has the highest energy density due to their long plateau at ~4.1 V and similar reversible. With increasing the rate from 1 C to 5 C, samples with more Fe amount have larger energy density, which is in accordance with the variation of capacity. That is because the longer plateau at ~4.1 V could not make compensation for the severe capacity reduction of samples with low Fe amount as the rates increase.

4. Conclusions

$LiMn_{0.9}Fe_{0.1}PO_4$ nanorods, nanoparticles and nanoplates were successfully synthesized under solvothermal condition at pH = 9, 11, and 12.5, respectively. The $LiMn_{0.9}Fe_{0.1}PO_4$ nanoplates show the highest rate capacity among the three samples, indicating the optimal pH value is 12.5. In order to further investigate the effect of Fe doping on the $LiMnPO_4$, a series of $LiMn_{1-x}Fe_xPO_4$ ($x = 0$, 0.1, 0.2, 0.3, 0.4 0.5) nanoplates were synthesized via the same routine at pH = 12.5. The Fe-substituted samples form a solid solution and the lattice parameters of which decrease with increasing Fe concentration. Electrochemical measurements revealed that cycling performance of $LiMn_{1-x}Fe_xPO_4$/C has been significantly improved as x rises. Fe-substitution also confers benefits to rate capability due to the suppression of Mn dissolution. Since materials studied here are all with *ca.* 2.7 wt. % carbon content which is the lowest among related papers, $LiMn_{0.5}Fe_{0.5}PO_4$/C nanoplates with good electrochemical properties prepared by a simple solvothermal method in this paper show as potential cathode materials for Li-ion batteries.

Acknowledgments

We are grateful for financial support from the Key Research Program of Chinese Academy of Sciences (Grant No. KGZD-EW-202-4), the Natural Science Foundation of Ningbo (Grant No. 2012A610126), the Key Technology R&D Program of Ningbo (2012B10021) and Ningbo Science and Technology Innovation Team (Grant No. 2012B82001).

References

[1] A.K. Padhi, K.S. Nanjundaswamy, J.B. Goodenough, J. Electrochem. Soc. 144 (1997) 1188–1194.
[2] L. Dimesso, C. Förster, W. Jaegermann, J.P. Khanderi, H. Tempel, A. Popp, J. Engstler, J.J. Schneider, A. Sarapulova, D. Mikhailova, L.A. Schmitt, S. Oswald, H. Ehrenberg, Chem. Soc. Rev. 41 (2012) 5068–5080.
[3] K. Zaghib, A. Mauger, C.M. Julien, J. Solid State Electrochem. 16 (2012) 835–845.
[4] A. Yamada, Y. Kudo, K.Y. Liu, J. Electrochem. Soc. 148 (2001) A747–A754.
[5] G.H. Li, H. Azuma, M. Tohda, J. Electrochem. Soc. 149 (2002) A743–A747.
[6] I.C. Jang, H.H. Lim, S.B. Lee, K. Karthikeyan, V. Aravindan, K.S. Kang, W.S. Yoon, W.I. Cho, Y.S. Lee, J. Alloys Compd. 497 (2010) 321–324.
[7] K. Zaghib, A. Mauger, H. Groult, J.B. Goodenough, C.M. Julien, Materials 6 (2013) 1028–1049.
[8] S. Ong, V. Chevrier, G. Ceder, Phys. Rev. B 83 (2011) 075112.
[9] S.L. Shang, Y. Wang, Z.G. Mei, X.D. Hui, Z.K. Liu, J. Mater. Chem. 22 (2012) 1142–1149.
[10] S.M. Oh, S.W. Oh, C.S. Yoon, B. Scrosati, K. Amine, Y.K. Sun, Adv. Funct. Mater. 20 (2010) 3260–3265.
[11] H.S. Fang, H.H. Yi, C.L. Hu, B. Yang, Y.C. Yao, W.H. Ma, Y.N. Dai, Electrochim. Acta 71 (2012) 266–269.
[12] Y.R. Zhang, Y.Y. Zhao, L.J. Deng, Ionics 18 (2012) 573–578.
[13] K. Zaghib, M. Trudeau, A. Guerfi, J. Trottier, A. Mauger, R. Veillette, C.M. Julien, J. Power Sources 204 (2012) 177–181.
[14] J. Yoshida, M. Stark, J. Holzbock, N. Hüsing, S. Nakanishi, H. Iba, H. Abe, M. Naito, J. Power Sources 226 (2013) 122–126.
[15] S. Liu, H.S. Fang, B. Yang, Y.C. Yao, W.H. Ma, Y.N. Dai, J. Power Sources 230 (2013) 267–270.
[16] H.L. Wang, Y. Yang, Y.Y. Liang, L.F. Cui, H.S. Casalongue, Y.G. Li, G.S. Hong, Y. Cui, H.J. Dai, Angew. Chem. Int. Ed. 50 (2011) 7364–7368.
[17] S.M. Oh, H.G. Jung, C.S. Yoon, S.T. Myung, Z.H. Chen, K. Amine, Y.K. Sun, J. Power Sources 196 (2011) 6924–6928.
[18] Z. Tan, P. Gao, F.Q. Cheng, H.J. Luo, J.T. Chen, H.H. Zhou, S.T. Tan, Funct. Mater. Lett. 4 (2011) 299–303.
[19] L. Damen, F.D. Giorgio, S. Monaco, F. Veronesi, M. Mastragostino, J. Power Sources 218 (2012) 250–253.
[20] R. von Hagen, H. Lorrmann, K.C. Moller, S. Mathur, Angew. Chem. Int. Ed. 2 (2012) 553–559.
[21] J. Zong, Q.W. Peng, J.P. Yu, X.J. Liu, J. Power Sources 228 (2013) 214–219.
[22] A. Yamada, S.-C. Chung, J. Electrochem. Soc. 148 (2001) A960–A967.
[23] J. Yao, S. Bewlay, K. Konstantionv, V. Drozd, R. Liu, X. Wang, H. Liu, G. Wang, J. Alloys Compd. 425 (2006) 362–366.
[24] J. Molenda, W. Ojczyk, J. Marzec, J. Power Sources 174 (2007) 689–694.
[25] D.Y. Wang, H. Buqa, M. Crouzet, G. Deghenghi, T. Drezen, I. Exnar, N. Kwon, J.H. Miners, L. Poletto, M. Grätze, J. Power Sources 189 (2009) 624–628.
[26] J. Hong, F. Wang, X.L. Wang, J. Graetz, J. Power Sources 196 (2011) 3659–3663.
[27] K. Saravanan, V. Ramar, P. Balaya, J.J. Vittal, J. Mater. Chem. 21 (2011) 14925–14935.
[28] L. Chen, Y.Q. Yuan, X. Feng, M.W. Li, J. Power Sources 214 (2012) 344–350.
[29] J. Kim, K.Y. Park, I. Park, J.K. Yoo, J. Hong, K. Kang, J. Mater. Chem. 22 (2012) 11964–11970.
[30] M. Jo, H.C. Yoo, Y.S. Jung, J. Cho, J. Power Sources 216 (2012) 162–168.
[31] K. Dokko, S. Koizumi, H. Nakano, K. Kanamura, J. Mater. Chem. 17 (2007) 4803–4810.
[32] Y.R. Wang, Y.F. Yang, Y.B. Yang, H.X. Shao, Solid State Commun. 150 (2010) 81–85.
[33] D.W. Choi, D.H. Wang, I.T. Bae, J. Xiao, Z.M. Nie, W. Wang, V.V. Viswanathan, Y.J. Lee, J.G. Zhang, G.L. Graff, Z.G. Yang, J. Liu, Nano. Lett. 10 (2010) 2799–2805.
[34] P. Barpanda, K. Djellab, N. Recham, M. Armand, J.M. Tarascon, J. Mater. Chem. 21 (2011) 10143–10152.
[35] N.H. Kwon, K.M. Fromm, Electrochim. Acta 69 (2012) 38–44.
[36] Z.H. Qin, X.F. Zhou, Y.G. Xia, C.L. Tang, Z.P. Liu, J. Mater. Chem. 22 (2012) 21144–21153.
[37] S.L. Yang, X.F. Zhou, J.G. Zhang, Z.P. Liu, J. Mater. Chem. 20 (2010) 8086–8091.
[38] L. Wang, F. Zhou, G. Ceder, Electrochem. Solid-State Lett. 11 (2008) A94–A96.
[39] K. Dokko, S. Koizumi, K. Sharaishi, K. Kanamura, J. Power Sources 165 (2007) 656–659.
[40] K. Dokko, T. Hachida, M. Watanabe, J. Electrochem. Soc. 158 (2011) A1275–A1281.
[41] Y.J. Zhu, C.S. Wang, J. Phys. Chem. C 115 (2011) 823–832.